Tomographic reconstruction of time-bin-entangled qudits

Samantha J. Nowierski, Neal N. Oza, Prem Kumar, and Gregory S. Kanter

Phys. Rev. A **94**, 042328 — Published 19 October 2016

DOI: 10.1103/PhysRevA.94.042328

Tomographic reconstruction of time-bin entangled qudits

Samantha J. Nowierski[1,2], Neal N. Oza[1], Prem Kumar[1,3], and Gregory S. Kanter[1]
[1] *Center for Photonic Communication and Computing, EECS Department, Northwestern University, 2145 Sheridan Road, Evanston, IL 60208-3118, USA*
[2] *Graduate Program in Applied Physics, Northwestern University, Evanston, IL 60208, USA*
[3] *Department of Physics and Astronomy, Northwestern University, 2145 Sheridan Road, Evanston, IL 60208-3112, USA*

We describe an experimental implementation to generate and measure high-dimensional, time-bin entangled qudits. Two-photon time-bin entanglement is generated via spontaneous four-wave mixing in single-mode fiber. Unbalanced Mach-Zehnder interferometers transform selected time-bins to polarization entanglement, allowing standard polarization-projective measurements to be used for complete quantum state tomographic reconstruction. Here, we generate maximally entangled qubits ($d = 2$), qutrits ($d = 3$), and ququarts ($d = 4$), as well as other phase-modulated non-maximally entangled qubits and qutrits. We reconstruct and verify all generated states using maximum likelihood estimation tomography.

I. INTRODUCTION

Entanglement is desirable for secure optical quantum communication (QC). To increase information throughput, it is useful to encode many qubits per photon using entangled states of dimension d (qudits) [1, 2]. High-dimensional entangled qudits ($d > 2$) also violate Bell's inequalities more than qubits ($d = 2$), making them potentially more useful for QC [3]. Various QC schemes also call for entangled qudits, such as quantum secret sharing [4]. The generation of entangled qudits can also be beneficial for fields outside of QC, e.g. quantum illumination and quantum contextuality [5, 6].

High-dimensional photonic entangled states require one to use a degree of freedom of large dimension. Polarization, commonly used for entangled qubits, cannot be used for higher dimensional entanglement alone as it is limited to two orthogonal bases. Degrees of freedom extendable to higher dimensions include spatial modes, orbital angular momentum (OAM) modes, temporal modes (time bin or time-energy), or a combination of such modes to generate hyperentanglement [7, 8]. Although OAM entanglement was verified up to $d = 100$ [9], OAM modes are fundamentally incompatible with low-loss single-mode fiber [10]. Additionally, they are prone to turbulence in free-space transport which can destroy entanglement and they typically require slow, complicated waveform transformations for measurement [11, 12]. In contrast, the temporal degree of freedom is highly compatible with fiber-based optical communication as dispersion-induced degradation can be controlled using different types of fiber. Time-binning also allows for high-speed generation which is essential for fast communication, and the ability to easily vary the dimensionality of the state which is essential for the quantum secret sharing scheme described in [4]. A linear optical quantum computing scheme was also proposed using time-bin-encoded photons [13].

Entanglement verification using witnesses [14] or interference techniques [15] are useful, but quantum state tomography (QST) is essential to determine the full quantum state and all encoded information. QST was previously demonstrated with entangled qudits using OAM modes (up to $d = 8$) spatial modes (up to $d = 3$), and time-energy modes (up to $d = 4$) [16–19]. To the best of our knowledge, time-bin QST has been previously demonstrated for qubits only [20–23].

Here, we present a scheme for performing a full QST of time-bin entangled qudits using polarization-projective measurements. We verify the generation of maximally entangled qubits, qutrits, and ququarts as well as other non-maximally entangled qubits and qutrits.

II. EXPERIMENTAL SETUP

A. Qudit generation

Time-bin entangled qubits are commonly generated using spontaneous parametric down-conversion (SPDC) [21, 24] and spontaneous four-wave mixing (SFWM) [25, 26]. Time-bin entangled qudits generated using SPDC were previously verified using interference techniques as well as by making Bell-type measurements [15, 27]. Here, we generate entangled photon pairs in the O-band (1260–1360 nm) using SFWM in single-mode fiber (SMF).

Figure 1 shows the experimental setup for time-bin entangled state generation. The pump at 1305 nm generates signal and idler photons pairs at 1306.5 nm and 1303.5 nm, respectively. This pair generation process is phase-matched in SMF and was previously developed in [28]. A pulsed pump generates these pairs in discrete time bins determined by the the pump's temporal shape. The O-band is desirable as it exhibits low transmission loss and low dispersion in communication-grade fiber.

A 10-GHz optical pulse stream at 1305 nm is first generated using a frequency comb source and pulse compression [29]. The frequency comb is created using a seed CW laser centered at 1305 nm followed by a phase modulator

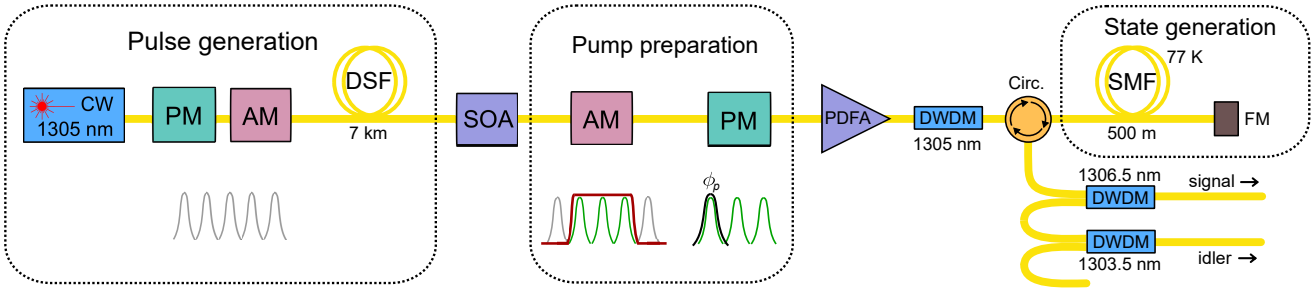

FIG. 1. Schematic of state generation. AM, amplitude modulator; Circ., circulator; DSF, dispersion-shifted fiber; DWDM, dense wavelength division multiplexer; FM, Faraday mirror; PDFA, Praseodymium doped fiber amplifier; PM, phase modulator; SOA, semiconductor optical amplifier. The DWDM bandwidth is 0.42 nm.

(PM) and amplitude modulator (AM) both driven at 10 GHz to form pulses. To further compress the pulses, the modulated light is sent into a 7-km spool of dispersion-shifted fiber (DSF) with a zero-dispersion wavelength of 1551 nm. The output pulses have a FWHM of 16 ps and are separated by 100 ps which defines the time bin separation.

We prepare the pump by pulse-picking d consecutive pulses at a rate of 50 MHz using an AM. The PM that follows allows a phase, $\phi_{p,j}$, to be applied to any given time bin j in order to generate phase-modulated entangled states. The pump is sent through a circulator and into a 500-m spool of SMF followed by a Faraday mirror (FM) that reflects the pulses back through the SMF to the circulator output and filters. We suppress Raman photon generation by cooling the fiber to 77 K using liquid nitrogen [30, 31]. The pump power is set to yield a pair production rate (PPR) of ≈ 0.04 per pulse to balance the competing desires of a high count rate and low multi-pair emissions.

Using a single pump, the following state is generated using SFWM,

$$|\psi_d\rangle = \sum_{j=0}^{d-1} b_j e^{i\phi_j} |j\rangle_s \otimes |j\rangle_i = \frac{1}{\sqrt{d}} \sum_{j=0}^{d-1} e^{i\phi_j} |jj\rangle , \quad (1)$$

where $\phi_j = 2\phi_{p,j}$. Therefore, without phases applied using the PM, we expect the generated state to take the form of a maximally entangled state $|\psi_{d,\max}\rangle = \frac{1}{\sqrt{d}} (|00\rangle + \ldots + |(d-1)(d-1)\rangle)$. The coherence time of the SFWM pump is 80 ns, which limits the generated state dimension to $d < 80$. The current setup allows for generation up to $d = 4$, but can be expanded to higher dimensions with additional pulse-picking electronics.

B. Polarization-based measurement

QST requires a complete set of measurements to be made on the state [32, 33]. In lieu of complex, direct high-dimensional time-bin-projective measurements, we use multiple two-dimensional polarization-projective measurements [34]. The projective measurements needed for each photon, for $t_a, t_b \in (0, \ldots, d-1)$, are $|t_a\rangle, |t_b\rangle, \frac{1}{\sqrt{2}} (|t_a\rangle + |t_b\rangle), \frac{1}{\sqrt{2}} (|t_a\rangle - |t_b\rangle), \frac{1}{\sqrt{2}} (|t_a\rangle + i\,|t_b\rangle)$, and $\frac{1}{\sqrt{2}} (|t_a\rangle - i\,|t_b\rangle)$. By mapping any two time bins onto orthogonal polarizations, i.e., $|t_a\rangle \rightarrow |H\rangle$ and $|t_b\rangle \rightarrow |V\rangle$, the time-bin projections correspond directly to H, V, D, A, R, and L polarization-projections [21]. Therefore, we can use established polarization-based techniques to make time-bin-projective measurements. All pairwise combinations of these measurements for each photon are made to obtain a complete QST.

We use a novel system composed of unbalanced Mach-Zehnder interferometers (UMZIs) and a high-speed optical switch to perform each time-bin-to-polarization transformation. Conversion of time-bin qubit entanglement to polarization entanglement was previously accomplished in [35] using free space optics. Here we make use of temporal-to-polarization conversion to perform a full quantum state tomography on high-dimensional time-bin entanglement. Figure 2 details the experimental method.

The signal and idler photons are sent into an UMZI, framed by a 50/50 beam splitter (BS) and a polarizing beam splitter (PBS). Half of the incoming light is therefore mapped to horizontal polarization H and half to vertical polarization V. The tunable optical delay (TOD) in one arm of the interferometer is set to change the delay by increments of 100 ps, which temporally superimposes two time bins of orthogonal polarization at the output. To stabilize the UMZI, a tap of the CW laser used to generate the entangled pairs is sent reverse-propagating through each UMZI via the second port of the PBS. A photodetector monitors this signal and provides feedback, through an Arduino-based PID circuit, to control a phase shifter. In this manner, the interferometer is phase-stabilized and locked to the source laser. The relative phase between each arm in the UMZIs fluctuates with a standard deviation of 1.5° when the arms are balanced, and increases to 2° when unbalanced by 300 ps.

Currently available single photon detectors cannot resolve pulses separated by 100 ps, thus we select which temporal superposition to measure using a cross-bar optical switch acting as a temporal shutter [36, 37]. This cross-phase modulation (XPM) based switch allows for simultaneous low-loss, low-noise, high-isolation, and fast

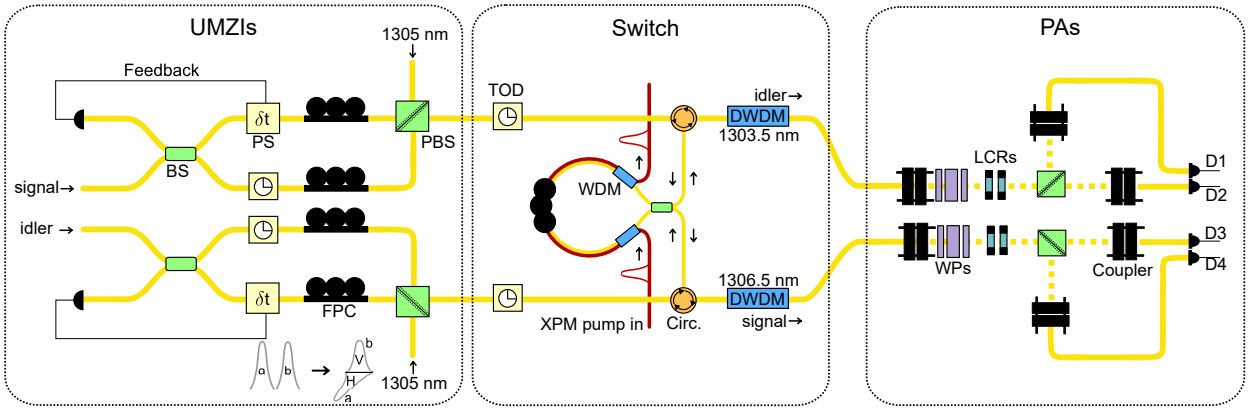

FIG. 2. Schematic of polarization-basis measurement setup with unbalanced Mach-Zehnder interferometers (UMZIs), switch, and polarization analyzers (PAs). BS, beam splitter; Circ., circulator; D, single photon detector; DWDM, dense wavelength division multiplexer; FPC, fiber polarization controller; LCR, liquid crystal retarder; PBS, polarizing beam splitter; PS, phase shifter; TOD, tunable optical delay; WDM, wavelength division multiplexer; WP, waveplate.

TABLE I. Measurement settings

$\|t_a\rangle, \|H\rangle$	$\|t_b\rangle, \|V\rangle$	TOD, UMZI (ps)	TOD, switch (ps)
$\|0\rangle$	$\|1\rangle$	100 ps	100 ps
$\|0\rangle$	$\|2\rangle$	200 ps	200 ps
$\|0\rangle$	$\|3\rangle$	300 ps	300 ps
$\|1\rangle$	$\|2\rangle$	100 ps	200 ps
$\|1\rangle$	$\|3\rangle$	200 ps	300 ps
$\|2\rangle$	$\|3\rangle$	100 ps	300 ps

manipulation and routing of our signal and idler photons. The XPM pump used has a FWHM of 16 ps. The pump is dual wavelength (1547.2 nm and 1550.9 nm) and cross-polarized to ensure polarization-independent switching. The switching window is configured to be 50 ps by using ≈ 20 meters of SMF in the switch. This window is sufficient to allow for only one temporal superposition to be transmitted while blocking the others, ensuring a two-dimensional measurement. The TOD at the output of each UMZI is used to adjust which superposition is transmitted through the switch. Table I lists the TOD settings needed for any given mapping for $d < 5$.

The selected photons are then routed to the polarization analyzers (PAs) for measurement. The PAs are comprised of a series of waveplates (WPs) for birefringence compensation and liquid crystal retarders (LCRs) followed by a PBS to make the required measurements for QST. The PAs are the only component of the experiment done in free-space. The use of electronically controlled LCRs instead of WPs speeds up measurement times. The single (S) and coincidence (CC) counts are recorded using four single photon detectors (SPDs), NuCrypt CPDS 1000-4, labeled as D_{1-4}. Accidental coincidence counts (ACC) are calculated for a given two detectors k and l as $ACC_{kl} = S_k \times S_l / N_G$, where N_G is the number of detector gates.

The total transmission after state generation until prior to detection, η_t, is 0.05 in both the signal and idler photon paths. The SPDs are set to have photon detection efficiencies, η_d, of 12–18% and have a dark count rate of $\approx 1 \times 10^{-4}$ per pulse. Additionally, approximately 1×10^{-4} noise photons per pulse are detected from amplified spontaneous emission from the XPM pump's EDFA and O-band anti-Stokes Raman photons generated in the switch by the XPM pump. The total background count probability per pulse (B) including detector dark counts and noise photons at each detector thus amounts to $\approx 2 \times 10^{-4}$.

III. RESULTS

We use maximum likelihood estimation (MLE) to reconstruct the states [38]. For each given two-dimensional superposition, we make 36 polarization-projective measurements to best account for varying detector efficiencies. Therefore the total number of measurements for any qudit tomography is $36 \times \binom{d}{2}^2$, which amounts to 36, 324, and 1296 measurements for qubit, qutrit, and ququart tomographies, respectively. Counts are recorded for a fixed $N_G = 800 \times 10^6$ (≈ 16 seconds) per measurement, which linearly scales the time for tomography with the number of measurements. The fiber's birefringence is accounted for using the WPs as well as computationally. The transmission of one time-bin superposition by the switch limits the number of measurements that can be taken in a given period of time, as only one time-bin superposition is transmitted at a given time. With the addition of another switch, and another set of four detectors, we would be able to measure two different two-dimensional projections simultaneously and reduce measurement time.

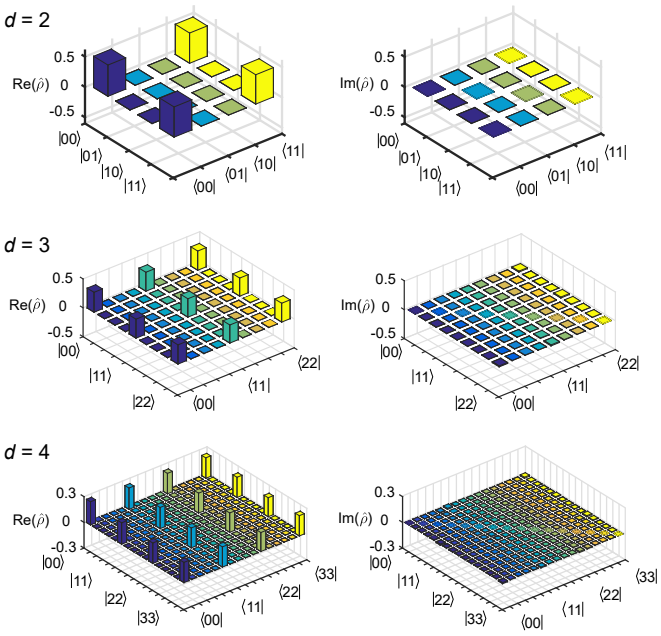

FIG. 3. Reconstructed maximally entangled qubit, qutrit, and ququart density matrices with accidental coincidences subtracted. The real and imaginary components of the density matrices are shown. Fidelity relative to a maximally entangled state is $99.3 \pm 0.5\%$, $97.0 \pm 0.4\%$, and $93.7 \pm 0.4\%$, respectively.

A. Maximally entangled qudits

Without applying phase shifts to any time bins using the PM (shown in Fig. 1), we generate maximally entangled qudits for $d = 2$, 3, and 4. The real and imaginary components of the reconstructed density matrices, $\hat{\rho}$, are shown in Fig. 3. We characterize the density matrices using fidelity, defined as

$$F(\hat{\rho}, \rho_{\text{ideal}}) = \left(\text{Tr} \left\{ \sqrt{\sqrt{\hat{\rho}} \rho_{\text{ideal}} \sqrt{\hat{\rho}}} \right\} \right)^2, \qquad (2)$$

relative to the expected density matrix, ρ_{ideal} [39]. With accidental-subtracted coincidences, the fidelity of each measured state relative to a maximally entangled state is $99.3 \pm 0.5\%$, $97.0 \pm 0.4\%$, and $93.7 \pm 0.4\%$, respectively. Error bars are calculated assuming Poisson counting statistics.

A summary of the fidelities of the reconstructed states for each dimension with varying amounts of background subtraction is shown in Fig. 4. The measured results are plotted along with the fidelity of a state that minimally violates Bell's inequalities [40]. Background-caused accidental counts (ACC_B) are calculated for each measurement using a given two detectors k and l as $ACC_{B,kl} = S_k \times B_l + S_l \times B_k - B_k \times B_l \times N_G$. Reconstruction after subtracting out the impact of all accidental coincidence counts or after subtracting out only background-caused accidental coincidences yields states

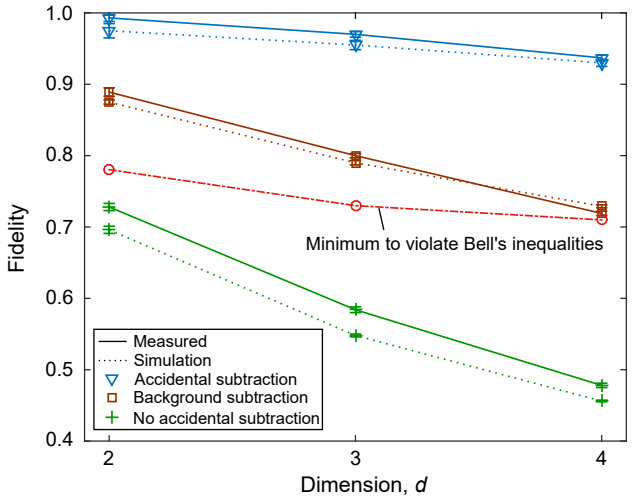

FIG. 4. Fidelity of reconstructed maximally entangled states with and without accounting for background photons (solid) as compared to simulation (dots). Theoretical minimal Bell's inequality violation (dash-dot), accidental subtraction (triangle), background subtraction (square), no subtraction (cross).

that exceed the minimum Bell state inequality threshold. As d increases, there is a decrease in fidelity with accidental-coincidences subtracted as a result of the low count rate, and long measurement times.

The combination of high end-to-end loss and fairly high background count levels currently limit the raw coincidence count performance. We can potentially in-

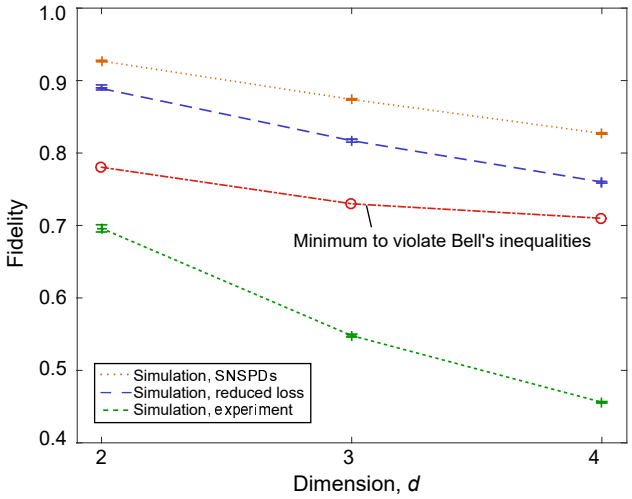

FIG. 5. Fidelity of simulated reconstructed maximally entangled qudits, without accidental-coincidences subtracted. Simulation using all experimental parameters (dash). Simulation with $\eta_t = 0.1$, and with superconducting nanowire single photon detector (SNSPDS) with $\eta_d = 0.75$, $B = 1 \times 10^{-4}$, and $PPR = 0.01$ (dots). Simulation with $\eta_t = 0.23$, $\eta_d = 0.15$, $B = 1.5 \times 10^{-4}$, and $PPR = 0.01$ (long dashes).

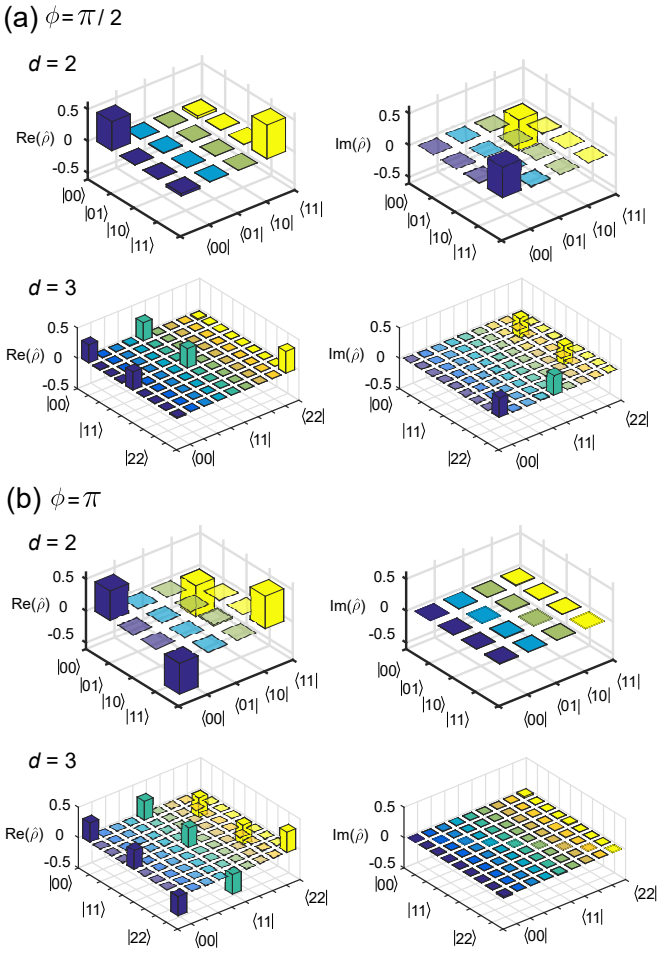

FIG. 6. Reconstructed qubit and qutrit density matrices when phases were applied to the pump using the PM with accidental coincidences subtracted. (a) $\phi = \pi/2$. Fidelities are $96.3 \pm 0.9\%$ and $94.7 \pm 0.7\%$ (b) $\phi = \pi$. Fidelities are $96.3 \pm 1.0\%$ and $94.0 \pm 0.8\%$.

crease the overall transmission by 3 dB in both the signal and idler path by splicing components that are currently connectorized, and reduce Raman generated background photon rate in half by changing the mean XPM pump wavelength from 1549 nm to 1562 nm. Figure 5 predicts the resulting performance with no background count subtraction if a superconducting nanowire single photon detector (SNSPD) with $\eta_d = 0.75$, a dark count rate of 5×10^{-5}, and $B = 1 \times 10^{-4}$ is used in such an experiment. Expected measured fidelities easily exceeds the Bell inequality threshold in this case. Also shown is the simulated performance using the experimental detectors, but with $\eta_t = 0.23$ and the longer XPM pump wavelengths yielding $B = 1.5 \times 10^{-4}$. These parameters again would allow the Bell inequality threshold to be exceeded.

B. Non-maximally entangled qudits

The pump PM allows various entangled states to be generated. By applying a phase to the appropriate pump pulse, we verified the generation of the following states using QST: $|\psi_{d,\phi}\rangle = \frac{1}{\sqrt{d}}\left(|00\rangle + \ldots + e^{i\phi}|(d-1)(d-1)\rangle\right)$, for $d = 2$ and 3, and $\phi = \pi/2$ and π. Our experiment allows for the application of a phase, any value up to π, to any time bin. We chose to apply the phases to the highest time bin for convenience.

Figure 6 plots the real and imaginary components of the reconstructed density matrices for the qubit and qutrit states listed above, with accidental coincidences subtracted. No parentheses indicate results with full accidental-coincidence subtraction and parentheses indicate results with background subtraction only. The measured fidelities were $96.3 \pm 0.9\%$ ($89.9 \pm 0.6\%$) and $96.3 \pm 1.0\%$ ($88.9 \pm 0.6\%$) for $|\psi_{2,\pi/2}\rangle$ and $|\psi_{2,\pi}\rangle$. For $|\psi_{3,\pi/2}\rangle$ and $|\psi_{3,\pi}\rangle$, the measured fidelities were $94.7 \pm 0.7\%$ ($82.3 \pm 0.6\%$) and $94.0 \pm 0.8\%$ ($81.9 \pm 0.5\%$). Generating these phase-modulated entangled states is useful for implementing the quantum secret sharing scheme described in [4].

IV. CONCLUSION

In conclusion, we showed the generation of various time-bin entangled qudit states, for $d = 2$, 3, and 4, using SFWM. An UMZI combined with a high-speed XPM-based optical switch mapped the multi-dimensional states onto a series of polarization states and enabled the use of standard polarization analyzers for QST. After taking into account background counts, we verified the generation of the maximally entangled qudits that exceeded the Bell's inequality threshold up to $d = 4$. To our knowledge, this is the first demonstrated QST of qutrit and ququart time-bin entangled states. We also were able to generate phase-modulated entangled qubit and qutrits with high fidelity. The use of electro-optic modulation to choose the state dimension and to apply phases to any time bin enables rapid variation in the entangled state generated, which is useful QC. With minor experimental changes, we expect to measure $d = 5$ entanglement as well. The number of measurements required for a full QST ultimately limits the highest dimensional state that can be measured using these methods.

ACKNOWLEDGMENTS

This research is supported in part by the ARO (Grant No. W911NF-12-1-0542). SJN is supported by the NSF Graduate Research Fellowship (Grant No. DGE-1324585). NNO was supported by the NSF Integrative Graduate Education and Research Traineeship (Grant No. DGE-0801685). Any opinion, findings, and conclusions or recommendations are those of the author(s) and do not necessarily reflect the views of the agencies listed above.

[1] J. Barreiro, T.-C. Wei, and P. Kwiat, Nature Physics **4**, 282 (2008).
[2] J. H. Shapiro, IEEE Journal of Selected Topics in Quantum Electronics **15**, 1547 (2009).
[3] D. Kaszlikowski, P. Gnaciński, M. Zukowski, W. Miklaszewski, and A. Zeilinger, Phys. Rev. Lett. **85**, 4418 (2000).
[4] H. Takesue and K. Inoue, Phys. Rev. A **74**, 012315 (2006).
[5] S. Lloyd, Science **321**, 1463 (2008).
[6] X. Zhan, X. Zhang, J. Li, Y. Zhang, B. C. Sanders, and P. Xue, Phys. Rev. Lett. **116**, 090401 (2016).
[7] J. T. Barreiro, N. K. Langford, N. A. Peters, and P. G. Kwiat, Phys. Rev. Lett. **95**, 260501 (2005).
[8] J.-W. Pan, Z.-B. Chen, C.-Y. Lu, H. Weinfurter, A. Zeilinger, and M. Żukowski, Rev. Mod. Phys. **84**, 777 (2012).
[9] M. Krenn, M. Huber, R. Fickler, R. Lapkiewicz, S. Ramelow, and A. Zeilinger, Proceedings of the National Academy of Sciences **111**, 6243 (2014).
[10] Y. Kang, J. Ko, S. M. Lee, S.-K. Choi, B. Y. Kim, and H. S. Park, Phys. Rev. Lett. **109**, 020502 (2012).
[11] S. Straupe and S. Kulik, Nature Photonics **4** (2010).
[12] S. Etcheverry, G. Caas, E. S. Gomez, W. T. Nogueira, C. Saavedra, G. B. Xavier, and G. Lima, Scientific Reports **3** (2013).
[13] P. C. Humphreys, B. J. Metcalf, J. B. Spring, M. Moore, X.-M. Jin, M. Barbieri, W. S. Kolthammer, and I. A. Walmsley, Phys. Rev. Lett. **111**, 150501 (2013).
[14] D. Chruściński and A. Rutkowski, The European Physical Journal D **62**, 273 (2011).
[15] H. de Riedmatten, I. Marcikic, V. Scarani, W. Tittel, H. Zbinden, and N. Gisin, Physical Review A **69**, 050304 (2004).
[16] M. Agnew, J. Leach, M. McLaren, F. S. Roux, and R. W. Boyd, Phys. Rev. A **84**, 062101 (2011).
[17] C. Bernhard, B. Bessire, T. Feurer, and A. Stefanov, Phys. Rev. A **88**, 032322 (2013).
[18] N. K. Langford, R. B. Dalton, M. D. Harvey, J. L. O'Brien, G. J. Pryde, A. Gilchrist, S. D. Bartlett, and A. G. White, Phys. Rev. Lett. **93**, 053601 (2004).
[19] W. M. Pimenta, B. Marques, T. O. Maciel, R. O. Vianna, A. Delgado, C. Saavedra, and S. Pádua, Phys. Rev. A **88**, 012112 (2013).
[20] S. X. Wang, C. Chan, P. Moraw, D. R. Reilly, J. B. Altepeter, and G. S. Kanter, Phys. Rev. A **86**, 042122 (2012).
[21] H. Takesue and Y. Noguchi, Opt. Express **17**, 10976 (2009).
[22] J. M. Donohue, M. Agnew, J. Lavoie, and K. J. Resch, Phys. Rev. Lett. **111**, 153602 (2013).
[23] H. Jayakumar, A. Predojevi, T. Kauten, T. Huber, G. S. Solomon, and G. Weihs, Nature Communications **7** (2014), 10.1038/ncomms5251.
[24] I. Marcikic, H. de Riedmatten, W. Tittel, H. Zbinden, M. Legré, and N. Gisin, Phys. Rev. Lett. **93**, 180502 (2004).
[25] H. Takesue, Opt. Express **14**, 3453 (2006).
[26] H. Takesue and K. Inoue, Phys. Rev. A **72**, 041804 (2005).
[27] T. Ikuta and H. Takesue, Phys. Rev. A **93**, 022307 (2016).
[28] M. A. Hall, J. B. Altepeter, and P. Kumar, Opt. Express **17**, 14558 (2009).
[29] R. Wu, V. R. Supradeepa, C. M. Long, D. E. Leaird, and A. M. Weiner, Opt. Lett. **35**, 3234 (2010).
[30] Q. Lin, F. Yaman, and G. P. Agrawal, Phys. Rev. A **75**, 023803 (2007).
[31] H. Takesue and K. Inoue, Opt. Express **13**, 7832 (2005).
[32] R. T. Thew, K. Nemoto, A. G. White, and W. J. Munro, Phys. Rev. A **66**, 012303 (2002).
[33] J. Altepeter, E. Jeffrey, and P. Kwiat (Academic Press, 2005) pp. 105 – 159.
[34] S. Nowierski, N. N. Oza, P. Kumar, and G. S. Kanter, *CLEO: 2015*, CLEO: 2015 , FTu2A.5 (2015).
[35] H. Takesue, K. Inoue, O. Tadanaga, Y. Nishida, and M. Asobe, Opt. Lett. **30**, 293 (2005).
[36] M. A. Hall, J. B. Altepeter, and P. Kumar, New Journal of Physics **13**, 105004 (2011).
[37] N. N. Oza, Y. P. Huang, and P. Kumar, IEEE Photonics Technology Letters **26**, 356 (2014).
[38] D. F. V. James, P. G. Kwiat, W. J. Munro, and A. G. White, Phys. Rev. A **64**, 052312 (2001).
[39] R. Jozsa, Journal of modern optics **41**, 2315 (1994).
[40] D. Collins, N. Gisin, N. Linden, S. Massar, and S. Popescu, Phys. Rev. Lett. **88**, 040404 (2002).